European Journal of Pharmaceutical Sciences 176 (2022) 106263

Contents lists available at ScienceDirect

European Journal of Pharmaceutical Sciences

journal homepage: www.elsevier.com/locate/ejps

Production, physicochemical investigations, antioxidant effect, and cellular uptake in Caco-2 cells of the supersaturable astaxanthin self-microemulsifying tablets

Wai Thet Aung [a,b], Hnin Ei Ei Khine [a,c], Chatchai Chaotham [c,d], Veerakiet Boonkanokwong [b,*]

[a] Graduate Program of Pharmaceutical Sciences and Technology, Faculty of Pharmaceutical Sciences, Chulalongkorn University, Bangkok 10330, Thailand
[b] Department of Pharmaceutics and Industrial Pharmacy, Faculty of Pharmaceutical Sciences, Chulalongkorn University, 254 Phayathai Road, Wang Mai, Pathum Wan, Bangkok 10330, Thailand
[c] Department of Biochemistry and Microbiology, Faculty of Pharmaceutical Sciences, Chulalongkorn University, Bangkok 10330, Thailand
[d] Center of Excellence in Cancer Cell and Molecular Biology, Faculty of Pharmaceutical Sciences, Chulalongkorn University, Bangkok 10330, Thailand

ARTICLE INFO

Keywords:
Astaxanthin
Self-microemulsifying tablets
Spray drying
Caco-2 cells
Antioxidant activity

ABSTRACT

The purpose of this study was to develop astaxanthin (AST)-loaded self-microemulsifying drug delivery system (SMEDDS) tablets and evaluate their physicochemical and biological properties. The optimized liquid (L)-AST SMEDDS formulation was composed of rice bran oil (33.67%), Kolliphor® RH 40 (34.70%), and Span® 20 (31.63%). Two types of hydrophilic polymers (hydroxypropyl methylcellulose, HPMC, and polyvinyl alcohol, PVA) solutions were selected as a precipitation inhibitor for AST and incorporated into L-AST SMEDDS to obtain supersaturation and enhance dissolution of AST. The formulation was then mixed with microcrystalline cellulose and subsequently transformed to solid S-AST SMEDDS particles using a spray dryer prior to direct compression into tablets. The HPMC AST SMEDDS tablet and PVA AST SMEDDS tablet were characterized for their physicochemical properties, dissolution, AST release, and stabilities. Moreover, the cellular uptake and antioxidant effect of AST SMEDDS tablets were evaluated in Caco-2 cells. With good tablet characters, both HPMC AST SMEDDS tablet and PVA AST SMEDDS tablet dissolution profiles were improved compared to that of raw AST. While initially less than 50% of AST released from HPMC AST SMEDDS tablet and PVA AST SMEDDS tablet in pH 1.2 medium, after 6 h more than 98% of AST releases in pH 6.8 were achieved which was similar to L-AST SMEDDS profile. Cellular antioxidant activities of L-AST SMEDDS and HPMC AST SMEDDS tablet & PVA AST SMEDDS tablet were significantly greater than pure AST powder. HPMC AST SMEDDS tablet showed better uptake and deeper penetration through Caco-2 cells than that in PVA AST SMEDDS tablet and pure powder. Our successfully developed AST SMEDDS tablets were demonstrated to be a potential platform to deliver highly lipophilic AST and improve permeation and bioavailability.

1. Introduction

Astaxanthin (AST) is a pigmented xanthophyll carotenoid that is abundantly found in natural sources including aquatic animals, some birds, and microorganisms (Shikov et al., 2020; Viera et al., 2018). AST has a variety of biological activities that are beneficial to health and thus it has been extensively consumed in recent years. To fulfill the industrial-scale manufacture and supply the market's high demand, AST has been successfully harvested from microalgae (*Haematococcus pluvialis*), mold (*Blakeslea trispora*), yeast (*Xanthophyllomyces dendrorhous*), and bacteria (*Agrobacterium aurantiacum*) (Capelli et al., 2019; Martínez-Delgado et al., 2017). The monoester conjugated natural AST was approved as a nutraceutical for humans by the United States Food and Drug Administration in late 1990s providing several health benefits (Yang et al., 2013).

AST possesses an antioxidant activity 10 and 100 times more than that of beta carotene and vitamin E, respectively (Sun et al., 2020; Yamashita, 2013). Owing to the strong antioxidant activity of AST, it has been demonstrated for numerous health benefits such as anti-aging, anti-tumor, anti-diabetes, anti-inflammation, ocular protection, neuroprotection, and relief on oxidative stress related diseases (Shikov et al., 2020; Yang et al., 2013). Therefore, AST has been widely used as dietary

* Corresponding author.
E-mail address: veerakiet.b@pharm.chula.ac.th (V. Boonkanokwong).

https://doi.org/10.1016/j.ejps.2022.106263
Received 25 April 2022; Received in revised form 24 June 2022; Accepted 15 July 2022
Available online 16 July 2022

supplements and nutraceuticals (Aung and Boonkanokwong, 2021; Grimmig et al., 2017; Zin and Boonkanokwong, 2021). However, AST, which has a molecular weight of 596.84 g/mol and a log *P* (octanol/-water) value of 13.27, exhibits poor water solubility limiting absorption and oral bioavailability. Furthermore, AST is highly susceptible to degradation due to the polyunsaturated structure (Ponto et al., 2021).

In recent years, a self-microemulsifying drug delivery system (SMEDDS) has been successfully employed to improve oral absorption of lipophilic compounds. This lipid-based delivery system is an isotropic mixture composed of oil, surfactant, and cosurfactant, which will subsequently produce self-assembling oil-in-water microemulsions after dilution with gastrointestinal (GI) fluids (Pouton, 2000). The fine droplet size of self-assembling microemulsions is a great contribution to an enhanced oral bioavailability (Wang et al., 2020). For oral administration, liquid SMEDDS has been commonly filled into soft or hard gelatin capsules to deliver an active substance into the body. Manufacturing cost, inefficiency of filling a drug with low loading capacity, drug precipitation, leaking through or interaction with the capsule shells, and patient inconvenience issues can be limitations for the liquid SMEDDS in capsules.

Therefore, a number of researchers have studied and fabricated solidified SMEDDS with various types of solid carriers to improve product stability, dosing accuracy, ease of handling, better patient compliance, and profitability of manufacturing business (Mandić et al., 2017). Various techniques including adsorption, wet granulation via fluid bed granulation (Mandić et al., 2020), spray drying (Kim et al., 2015), freeze drying (Bi et al., 2016), and melt extrusion/granulation (Silva et al., 2018) are commonly chosen to perform solidification of self-emulsifying powders, pellets, granules, or tablets. Among these techniques, co-spray drying of SMEDDS with a solid carrier is extensively employed in the industry as it is a cost-effective one-step process for manufacturers. Moreover, it is suitable for drying thermolabile bioactive molecules due to rapid exposure to heat and quick evaporation of the liquids transforming to the dried powders within milliseconds.

Nevertheless, a bioactive compound with poor solubility and permeability often precipitates after dilution in the GI tract impairing the dissolution profile and absorption of the substance. Large amounts of surfactants in SMEDDS are required to remain the solubilized state of the compound while unwanted GI irritation may occur. In recent years, SMEDDS has been increasingly incorporated with hydrophilic polymeric precipitation inhibitors (PPIs) as polymers can achieve the "spring and parachute" effect on the active ingredient. Basically, the hydrophilic polymers used in the SMEDDS can maintain a meta-stable state of the solubilized compound and allow an appropriate duration of absorption (Quan et al., 2017; Singh et al., 2021) For instance, Kim et al. (2015) developed solid dutasteride SMEDDS by adding HPMC and Soluplus® as precipitation inhibitors to the conventional liquid SMEDDS. Higher oral bioavailability in rats was obtained from both Soluplus® and HPMC formulations compared to dutasteride raw powder, dutasteride-loaded SMEDDS without polymers, and the commercial product. Recent studies have clearly demonstrated that hydrophobic drugs such as dutasteride (Kim et al., 2015), fenofibrate (Quan et al., 2017), and valsartan (Yeom et al., 2017) were successfully incorporated into supersaturable SMEDDS using PPIs to maintain supersaturation after dispersion and thus enhance absorption and oral bioavailability.

According to our previous research (Aung and Boonkanokwong, 2021), a liquid self-microemulsifying drug delivery system (L-SMEDDS) containing rice bran oil, Kolliphor® RH 40, and Span® 20 was successfully developed by the design of experiment approach and the optimization technique, and AST was incorporated into the L-SMEDDS formulation. Still, AST SMEDDS in a tablet dosage form containing a hydrophilic PPI has not been developed and studied yet. In this work, L-AST SMEDDS was blended with hydrophilic polymer solutions and a solid carrier. Based on our previous results (Aung and Boonkanokwong, 2022), two types of polymers chosen for inhibition of AST precipitation were cellulose polymer (hydroxypropyl methylcellulose, HPMC) and synthetic vinyl polymer (polyvinyl alcohol, PVA) in order to increase the apparent AST solubility, maintain AST supersaturation state in the formulations, and enhance AST bioavailability. Subsequently, the mixture of supersaturable L-AST SMEDDS and polymer solution forming a self-assembling microemulsion was blended with a water-insoluble solid carrier (microcrystalline cellulose, MCC) and was transformed into solidified powder (S-AST SMEDDS) using a spray drying method. The resulting spray-dried S-AST SMEDDS powder was further blended with other excipients prior to direct compression to produce AST SMEDDS tablets for better product stability and patient compliance. Spray-dried S-AST SMEDDS powders and AST SMEDDS tablets were characterized for their morphologies and physicochemical properties. The effect of different types of the hydrophilic polymers incorporated into the AST SMEDDS tablets was evaluated. This research was aimed to improve *in vitro* dissolution as well as cellular antioxidant activity and uptake of AST SMEDDS tablets compared to L-AST SMEDDS and AST raw powder.

2. Materials and methods

2.1. Materials

2.1.1. Chemicals

Astaxanthin (CAS Number: 472-61-7) with at least 98% purity was purchased from Hangzhou DayangChem Co., Ltd. (Hangzhou, China). A food-grade rice bran (RB) oil was purchased from a local supermarket in Bangkok, Thailand. Kolliphor® RH 40 and Span® 20 were imported from BASF (Germany) and TCI (Tokyo Chemical Industry Co., Ltd., Japan), respectively. Microcrystalline cellulose (MCC; Avicel® PH-101) and hydroxypropyl methylcellulose (HPMC, E grade; HPMC-E5) were imported by Onimax Co., Ltd. (Thailand). Polyvinyl alcohol (PVA 8/88) was bought from Merck KGaA (Darmstadt, Germany). 1,1-diphenyl-2-picryl-hydrazil (DPPH), N-acetyl-L-cysteine (NAC), 2′,7′-dichlorofluorescin diacetate ($DCFH_2$-DA), dimethyl sulfoxide (DMSO), and coumarin 6 (C6) were purchased from Sigma-Aldrich (St. Louis, MO, USA). 3-(4,5-dimethylthiazol-2-yl)-2,5-diphenyltetrazolium bromide (MTT, Invitrogen™) and Hoechst33342 (Invitrogen™) were purchased from Thermo Fisher Scientific. HPLC-grade organic solvents including acetonitrile, dichloromethane, and methanol were purchased form Honeywell® (Republic of Korea).

2.1.2. Culture of Caco-2 cells

Human intestinal epithelial Caco-2 cells (ATCC® HTB-37) was purchased from the American Type Culture Collection (ATCC), Manassa, VA, USA. The cells were cultured in Dulbecco's modified eagle medium (DMEM; Gibco, Gaithersburg, MA, USA) containing 20% fetal bovine serum (FBS), 100 units/mL of penicillin/streptomycin, and 2 mmol/L of L-glutamine (Gibco, Gaithersburg, MA, USA). The cells were incubated at 37 °C in a humidified atmosphere of 5% CO_2 condition by replenishing the growth medium every three days (Thongrangsalit et al., 2015).

2.2. Preparation of solid AST SMEDDS (S-AST SMEDDS) using spray drying

The liquid (L)-AST SMEDDS was firstly prepared according to our previous study in which a mixture design was used to optimize the composition of the SMEDDS formulation examining on two main responses (i.e., the equilibrium solubility of AST in SMEDDS and the droplet size of the self-assembling microemulsions obtained from L-AST SMEDDS). Based on the results from an experimental design using a desirability function, the optimized L-SMEDDS was composed of rice bran oil (33.67% w/w), Kolliphor® RH 40 (34.70% w/w), and Span® 20 (31.63% w/w) (Aung and Boonkanokwong, 2021). The equilibrium solubility of AST in this optimized L-SMEDDS formulation was shown to be 404.80 ± 5.76 μg/mL, and the average droplet size of self-microemulsions obtained from the optimized L-SMEDDS was

measured as 40.79 ± 3.11 nm. Moreover, the solubility of AST in the optimized L-SMEDDS in presence of the same polymers (HPMC and PVA) used in this current work had been studied in our previous work (Aung and Boonkanokwong, 2022). It was found that these polymeric precipitation inhibitors had the ability to increase AST solubility in SMEDDS approximately 5 times greater than that in the condition without a polymer and to maintain AST concentration in the optimized L-AST SMEDDS above its supersaturation state for a certain period of time.

To prepare S-AST SMEDDS, firstly, 40 mg of AST was added into 5 g of L-SMEDDS and sonicated for 30 min to get a homogenous dispersion of the astaxanthin-loaded supersaturated SMEDDS (AST-Su-SMEDDS) which was subsequently dispersed in water (50 mL) until the clear reddish microemulsion was obtained. Then, polymer solutions were separately prepared by dissolving 5 g of HPMC E5 or 5 g of PVA 8/88 in 50 mL of water. A solid carrier, MCC 101 (7.5 g), was dispersed in the mixture of a self-microemulsion and a polymer solution, which was then stirred under a constant speed of ~250 rpm for 30 min to achieve a homogenous suspension and adjusted with water to get 10% w/v feeding suspension. The prepared suspension was solidified into spray-dried S-AST SMEDDS powders using a mini spray dryer (Büchi™ B90, Switzerland) under the following controls: inlet temperature ~105 °C, outlet temperature 55–60 °C, feeding pump rate 4–5 mL/min, and atomizing pressure 301–414 L/h.

2.3. Characterization of S-AST SMEDDS

2.3.1. Particle analysis of S-AST SMEDDS

Particle-size distribution (PSD) of the spray-dried powder was examined by the Morphologi 4-ID (Malvern Instruments Ltd, Worcestershire, UK) particle analyzer. For each measurement, the powder was dispersed on a glass plate using dispersion pressure of 4 bar. The number of individual particles was counted within the area of 20 mm × 20 mm, and particles' sizes were presented as circular equivalent (CE) diameter (in μm). The distribution width was represented by a span value which could be calculated from the following equation (Eq. (1)).

$$\text{Span} = \frac{(D_{90} - D_{10})}{D_{50}} \quad (1)$$

where D_{90}, D_{50}, and D_{10} are the diameters based on the percentage (90%, 50%, and 10%, respectively) of the powder sample that has a smaller particle size.

2.3.2. Solid state characterization of S-AST SMEDDS

Chemical compatibility between AST and other excipients in the spray-dried SMEDDS powder was assessed by using Fourier transform infrared (FTIR) spectroscopy with attenuated total internal reflection (Omnic™ software, Nicolet iS10, Thermo Scientific, Waltham, MA USA). FTIR spectra of the S-AST SMEDDS samples were recorded within the range of 4000–650 cm^{-1} with 64 scan/measurement at a 4 cm^{-1} resolution. Furthermore, transformation of AST crystallinity in the developed S-AST SMEDDS was determined by the powder X-ray diffractometer (PXRD; Miniflex600, Rigaku Corporation, Tokyo, Japan) conducted with monochromatic Cu-K α-radiation using 15 mA and 30 kV at the angular range from 3° to 40° (2θ) with 5°min^{-1} increment. Additionally, the thermal behavior of S-AST SMEDDS compared to AST raw material was investigated by differential scanning calorimetry (DSC 822, STAR system, Mettler Toledo, Greifensee, Switzerland). Each sample was weighed and sealed in an aluminum crucible before heated under a dry nitrogen atmosphere (flow rate of 15 mL/min) from temperature of 25 °C to 250 °C and with the heating rate of 10 °C min^{-1} where an empty pan was used as a reference (Su et al., 2021).

2.4. Production of AST SMEDDS tablets

A formulation of AST SMEDDS tablets is shown in Table 1, and each tablet contains 1 mg equivalent weight of AST. S-HPMC AST SMEDDS was used to produce HPMC AST SMEDDS tablets, and similarly S-PVA AST SMEDDS was made to PVA AST SMEDDS tablets. Firstly, all excipients were passed through the No. 40 mesh (425 μm sieve opening) to break any agglomerates or lumps. The spray-dried S-AST SMEDDS powders were manually blended with MCC and Aerosil® 200 in a brown bottle for 10–15 min, then mixed with croscarmellose sodium for another 5 min, and subsequently blended with stearic acid for 5 min prior to compression. The homogeneously blended mixtures were directly compressed into tablets (total weight of 1 g per tablet) with round flat-faced punches (20.0 mm in diameter) and a die by using the Manesty Model Type F3™ tablet press machine (Manesty machines Ltd., Liverpool, England) at a fixed compression force of 47–50 kN.

2.5. Evaluation of physicochemical properties of AST SMEDDS tablets

Physical (diameter, thickness, weight, hardness, and friability) and chemical (AST content) properties of the AST SMEDDS tablets for both formulas were evaluated according to the USP guideline for solid dosage forms (United States Pharmacopeia, 2015). All tablets were weighed using the 3-digit Mettler Toledo ME303 balance (Mettler Toledo, Switzerland). For diameter and thickness of the tablets, a digital vernier caliper was used to record the values. Tablet hardness and friability were measured by a tablet hardness tester (Schleuniger-2E, Switzerland) and the ERWEKA type-TAR 10 friability tester (ERWERKA GmbH, Langen, Germany), respectively. For determination of reconstitution properties of the self-assembling microemulsions, AST SMEDDS tablets were disintegrated and dissolved in purified water (250 mL) stirred at 100 rpm at 37 °C for more than 30 min until the tablets were completely dispersed and self-microemulsions formed. Supernatant was taken to measure the droplet size, polydispersity index (PDI), and zeta potential of the self-assembling microemulsions (Thongrangsalit et al., 2015). To determine AST content, HPLC analysis was carried out at the wavelength (λ) of 474 nm using Agilent LC: 1260 Infinity II system (Agilent, Santa Clara, USA) composed of a quaternary pump, an autosampler, and a diode array detector. A slight modification of HPLC separation was

Table 1
Formula of HPMC AST SMEDDS tablet and PVA AST SMEDDS tablet directly compressed from spray-dried S-HPMC AST SMEDDS powder and spray-dried S-PVA AST SMEDDS powder, respectively.

Composition	Amount	
Composition of L-SMEDDS	**Amount (%w/w)**	
Rice bran oil	33.67	
Kolliphor® RH40	34.70	
Span® 20	31.63	
Ingredient of spray-dried powder	**S-HPMC AST SMEDDS (%w/w)**	**S-PVA AST SMEDDS (%w/w)**
AST	0.23	0.23
L-SMEDDS	28.34	28.34
Hydroxypropyl methylcellulose (HPMC)	28.57	-
Polyvinyl alcohol (PVA)	-	28.57
Microcrystalline cellulose (MCC) 101	42.86	42.86
Ingredient of AST SMEDDS tablet	**HPMC AST SMEDDS tablet (%w/w)**	**PVA AST SMEDDS tablet (%w/w)**
S-HPMC AST SMEDDS	43.75	-
S-PVA AST SMEDDS	-	43.75
Microcrystalline cellulose (MCC) 101	52.25	52.25
Aerosil® 200	1.00	1.00
Croscarmellose sodium	2.00	2.00
Stearic acid	1.00	1.00

performed based on the previous study (Tzanova et al., 2017). The mobile phase methanol–acetonitrile–water (94:3:3 by volume) at 1.0 mL/min flow rate using an isocratic elution mode passed through the C18 column Ultisil® XB-C18 (5 μm; 250 × 4.6 mm) maintained at 25 °C. AST content was calculated from the calibration curve which was validated prior to sample analysis.

2.6. In vitro dissolution study

Cumulative release profiles of AST raw material, L-AST SMEDDS, HPMC AST SMEDDS tablets, and PVA AST SMEDDS tablets were conducted by using the USP type-II apparatus (Varian VK7000; Agilent Technologies, USA). Pure AST powder (1 mg) and L-AST SMEDDS (containing 1 mg of AST) were filled into hard gelatin capsules before they were put into the medium. Each AST SMEDDS tablet containing 1 mg of AST was placed directly in the dissolution medium. The samples were dispersed in 250 mL of two types of dissolution media to mimic *in vivo* condition, simulated gastric fluid (pH 1.2) and simulated intestinal fluid (pH 6.8) without enzymes at 37.0 ± 0.5 °C, and agitated with a constant rotating speed of 100 rpm. Samples were withdrawn at specific time points (15, 30, 60, 90, 120, 180, 240, 360, and 480 min) and replaced with the same volume of a fresh medium. Samples in a pH 1.2 medium were collected from the time points 0 to 120 min, and subsequently the dissolution medium was changed to pH 6.8 and the samples were collected from the time points 120 to 480 min. Data for the two-medium sequential dissolution profiles were plotted. The taken sample was dissolved in the organic solvent mixture of dichloromethane and methanol (1:1 by volume) to extract AST from the dissolution medium, and then after filtration with a syringe filter AST content was measured by an HPLC instrument at $\lambda = 474$ nm as described earlier (Mao et al., 2019; Tzanova et al., 2017).

2.7. In vitro cellular antioxidant activity of AST SMEDDS tablets

To investigate the cellular antioxidant activity of AST, the fluorescence probe $DCFH_2$-DA assay was performed as described by Dai et al. (2020) with slight modifications. Caco-2 cells were seeded in the 96-well plate at density of 1×10^4 cells/well for overnight. The cells were treated with various dilutions (1:1000, 1:500, and 1:250) of pure AST powder, L-AST SMEDDS, HPMC AST SMEDDS tablet, and PVA AST SMEDDS tablet for 24 h. NAC (5 mM) and H_2O_2 (100 mM) solutions were used as positive and negative controls. After incubation, the cells were washed with PBS (pH 7.4) and treated with 100 μL of $DCFH_2$-DA (10 μM) for 30 min in the dark place. Then, $DCFH_2$-DA solution was removed, and the cells were washed and immersed with PBS (pH 7.4). The cellular reactive oxygen species (ROS) level was detected by a fluorescence microplate reader (CLARIOstar, BMG LABTECH, Allmendgrün, Ortenberg, Germany) at emitted and excited wavelengths of 535 nm and 485 nm, respectively. The results were expressed as percentage of DCF (ROS) level, and the non-treated control was considered to be 100%.

2.8. Detection of cellular uptake by fluorescence staining

Qualitative cellular uptake of coumarin 6 (C6), a chemical fluorescent hydrophobic compound used as a representative of AST in this study, was assessed by co-staining with Hoechst33342 and C6. In a 6-well plate, Caco-2 cells were seeded at the density of 1×10^4 cells/mL for 7 days. The culture medium was replaced with Hanks' balanced salt solution (HBSS; Gibco, Gaithersburg, MA, USA) and stabilized for 30 min at 37 °C. Afterward, the cells were treated with C6-loaded samples (1:250) for 2 h and 4 h. At the indicated time point, the monolayers were fixed with 70% ethanol for 20 min at room temperature and washed again with HBSS solution. For visual observation on localization of C6 in Caco-2 cells, the cell nuclei were stained with Hoechst33324 dye for 30 min, and then cells were observed under an inverted fluorescence microscope (Olympus IX51 with DP70, Olympus Corp., Shinjuku-ku, Tokyo, Japan). For quantitation of C6 cellular uptake, the cells were treated with C6-loaded samples (1:250) and incubated for 1 h, 2 h, and 4 h. After predetermined time, the fluorescence intensity of C6 within the cells was analyzed by a fluorescence microplate reader ($\lambda_{ex} = 485$ nm and $\lambda_{em} = 528$ nm). The fluorescence intensity ratio of treated cells to un-treated cells was calculated for the cellular uptake efficiency (Joshi et al., 2016; Wang et al., 2017).

2.9. Detection of cellular uptake by flow cytometry

Flow cytometry analysis was further performed to confirm the uptake of C6-loaded samples in Caco-2 cells. The cells were cultured at the density of 1×10^5 cells/mL in a 6-well plate. The cells were incubated with or without C6 and C6-loaded samples (1:250) for 4 h. Then, the monolayers were washed with HBSS solution three times to remove the excess dye. The cells were detached and centrifuged at 5000 rpm (4 °C) to collect the pellets. After that, the single cell suspensions were made by adding 500 μL of HBSS. The C6-associated fluorescence intensity was measured by the Guava easyCyte flow cytometer using InCyte 3.3 software (EMD Millipore, Billerica, MA, USA) (Joshi et al., 2016).

2.10. AST cellular uptake assay

Cellular uptake of AST in Caco-2 cells was determined by an HPLC analysis based on the reported method from Shen et al. (2019). After seeding Caco-2 cells (5×10^5 cells/well) in 6-well plates, the cells were incubated at 37 °C under 5% CO_2 for 7 days. The culture medium was removed and replaced with an HBSS solution. Cells treated only with the HBSS solution were used as a control. Caco-2 cells were treated with the sample (250-time diluted solution of AST raw material, L-AST SMEDDS, HPMC AST SMEDDS tablet, or PVA AST SMEDDS tablet) for 4 h. After a 4-h incubation, the medium was removed, and the cells were washed three times with an HBSS solution. The cells were collected and lysed, and then cellular AST was extracted with dichloromethane:methanol mixture (1:1 v/v) prior to determination of the uptake AST content by the HPLC analysis at $\lambda = 474$ nm as previously described in Sections 2.5 and 2.6.

2.11. Stability of AST SMEDDS tablets

Stability study of the HPMC AST SMEDDS tablets and PVA AST SMEDDS tablets were performed under two different conditions (30 ± 2 °C/ RH 65 ± 5% and 40 ± 2 °C/ RH 75 ± 5%) for different storage time periods (0, 1, 2, and 3 months) (ICH, 2003). After the stability testing, the HPMC AST SMEDDS tablets and PVA AST SMEDDS tablets were measured for some physicochemical properties and reconstituted in purified water to form self-assembling microemulsions as described in the Evaluations of Physicochemical Properties of AST SMEDDS Tablets Method Section to measure changes in droplet size, PDI, zeta potential, and AST content of the self-microemulsions. The AST contents in SMEDDS tablets were determined over a period upon different storage conditions.

2.12. Statistical analysis

Statistical analyses on self-microemulsions' properties assembled from AST SMEDDS tablets, dissolution studies, and cell-based studies were performed using a statistical program SPSS (version 17.0, SPSS Inc., Chicago, IL, USA). Triplicate measurements on each experiment were carried out. One-way ANOVA was used to compare the mean values of analyses, and the results were presented as mean ± standard deviation (SD). To consider statistical significance, the differences in all analyses must be $p < 0.05$.

3. Results and discussion

3.1. Characterization of S-AST SMEDDS

3.1.1. Particle size and PSD of S-AST SMEDDS

Optimizing the spray drying process parameters and controlling them within a design space were extremely important to obtain the spray-dried products with desired quality attributes. In this study, to avoid over heating of AST and to stabilize the microemulsion system, various process parameters of spray drying were preliminarily screened under 120 °C for the inlet temperature and 60 °C for the outlet temperature using water as a vehicle. Particle-size distribution of the resulting spray-dried powders was greatly influenced by the atomization condition, polymer solution concentration, and surface tension of the samples. From particle analysis by microscopic optics using a static automated imaging system, an average particle size of S-HPMC AST SMEDDS was 9.88 ± 0.24 μm with a span value 1.67 ± 0.08, and S-PVA AST SMEDDS was 17.66 ± 1.48 μm with a span value 1.65 ± 0.43. Although a reasonably large particle size was required to achieve good flowability of the spray-dried powder in order to further compress into tablets, fine particles produced from a lab-scale spray dryer in our case could be acceptable. Larger particles could be also obtained by using large-scale spray dryers producing larger atomized droplets and with greater drying capacity (Al-Zoubi et al., 2021; Shepard et al., 2020). Owing to the span value less than 2% for each formulation, PSD was considerably low for S-AST SMEDDS powders. It could be expected of good flow behavior and uniformity of content in the formulations. Surface morphology of the spray-dried S-AST SMEDDS particles was further studied by a scanning electron microscope and presented in Fig. S1 in the attached Supplementary Material file.

3.1.2. Solid state characterization of S-AST SMEDDS

To assess chemical interactions, crystallinity, and thermotropic phase behaviors of AST and other excipients especially the selected polymers in the spray-dried SMEDDS powder formulations, FTIR, PXRD, and DCS were employed. The FTIR spectra recorded for pure AST

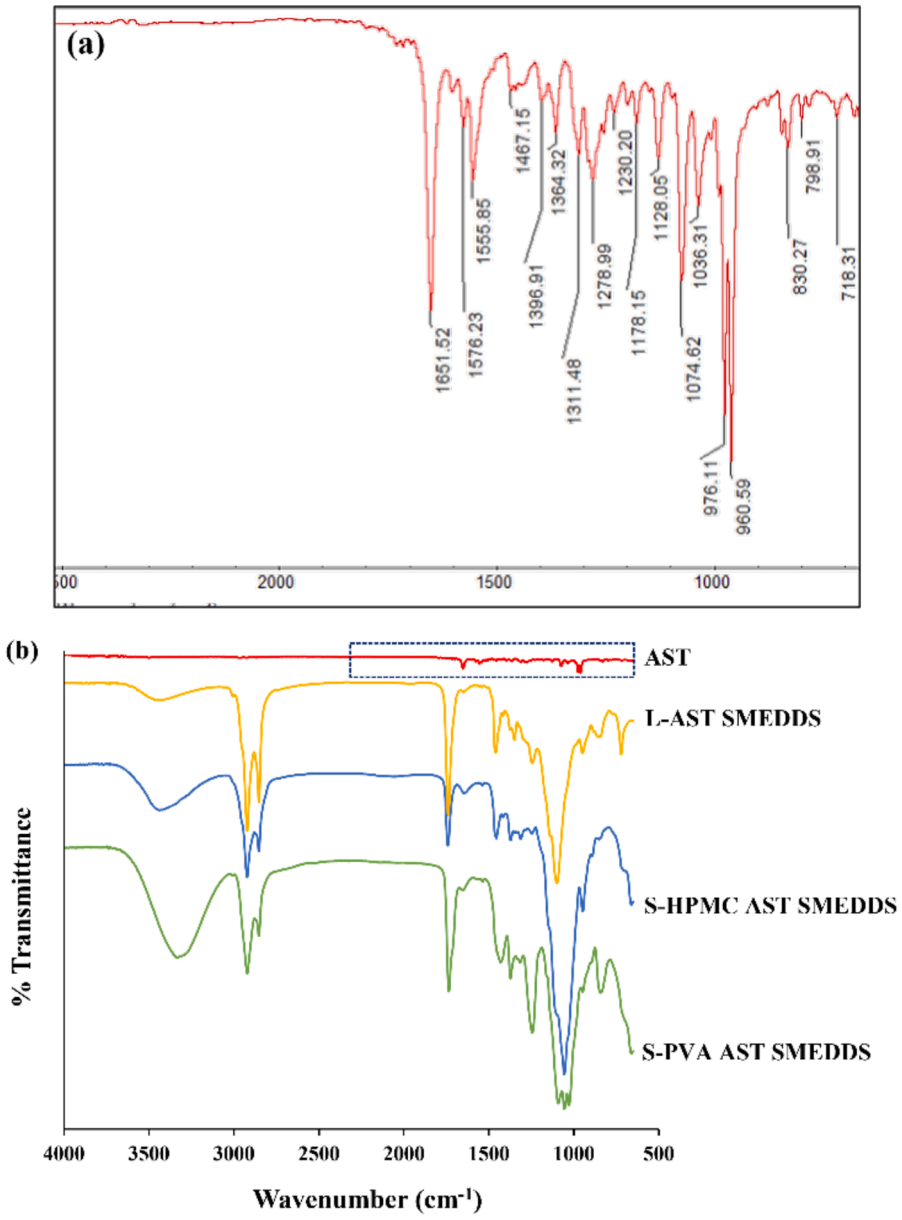

Fig. 1. Fourier transform infrared spectra: (a) AST raw material and (b) overlaid spectra of AST raw material, L-AST SMEDDS, S-HPMC AST SMEDDS, and S-PVA AST SMEDDS.

powder, L-AST SMEDDS, S-HPMC AST SMEDDS, and S-PVA AST SMEDDS were shown in Fig. 1. The characteristic peaks of AST were observed at 1652 cm^{-1} (C═O stretching), 1556 cm^{-1} (C═C stretching in the ring), and 960 cm^{-1} (C—H in the C and C conjugated system) as shown in Fig. 1 (a) (Hu et al., 2019). For the spectrum of L-AST SMEDDS containing rice bran oil, Kolliphor® RH 40, and Span® 20 shown in Fig. 1 (b), aliphatic O—H stretching at 3445 cm^{-1}, the bi-fork structure of the aliphatic C—H group stretching at 2852 cm^{-1} and 2921 cm^{-1}, ester (C═O vibration) absorption at 1738 cm^{-1}, and C═C vibration at 1654 cm^{-1} were mainly associated with triglycerides and unsaturated fatty acids of the vegetable oil and surfactants (Badria et al., 2020; Vlachos et al., 2006). In general, similar peaks and patterns were also observed in S-HPMC AST SMEDDS and S-PVA AST SMEDDS spectra due to the same SMEDDS composition as in L-AST SMEDDS. The small intensity peak at the region around 843 cm^{-1} (C—H group of neighboring aromatic ring of L-AST SMEDDS) and the sharp peak at 1240 cm^{-1} (C—C bonds vibration of the hydrocarbon skeletons of L-AST SMEDDS) occurred in S-PVA AST SMEDDS), but those of S-HPMC AST SMEDDS and L-AST SMEDDS were not clearly observed. Additionally, the scissoring vibrations of $–CH_2–$ and $–CH_3$ were also observed at 1460 cm^{-1} and 1370 cm^{-1}, respectively (Irnawati et al., 2019). It was shown that no additional characteristic peaks in the S-AST SMEDDS spectra compared to L-AST SMEDDS. However, when comparing S-HPMC AST SMEDDS and S-PVA AST SMEDDS, peak intensities (%transmittance) and peak shifts in the range of 3000–3600 cm^{-1} and at 1240 cm^{-1} of S-PVA AST SMEDDS were generally larger than those of S-HPMC AST SMEDDS, which were likely related to the physical interaction between PVA and L-AST SMEDDS in the encapsulation process. In addition, the intensity changes in both spectra of S-HPMC AST SMEDDS and S-PVA ASTSMEDDS could be attributed to presence of various interactions between L-AST SMEDDS and PPIs such as hydrogen bonds, van der Waals forces, or dipole interactions (Badria et al., 2020). These results suggested that AST was successfully incorporated in the spray-dried S-SMEDDS powders and that no chemical incompatibility issues between AST and excipients used in the formulations were significantly observed due to no additional peaks in all spectra.

The powder X-ray diffraction patterns of AST raw material, S-HPMC AST SMEDDS, and S-PVA AST SMEDDS were exhibited in Fig. 2 (a). A

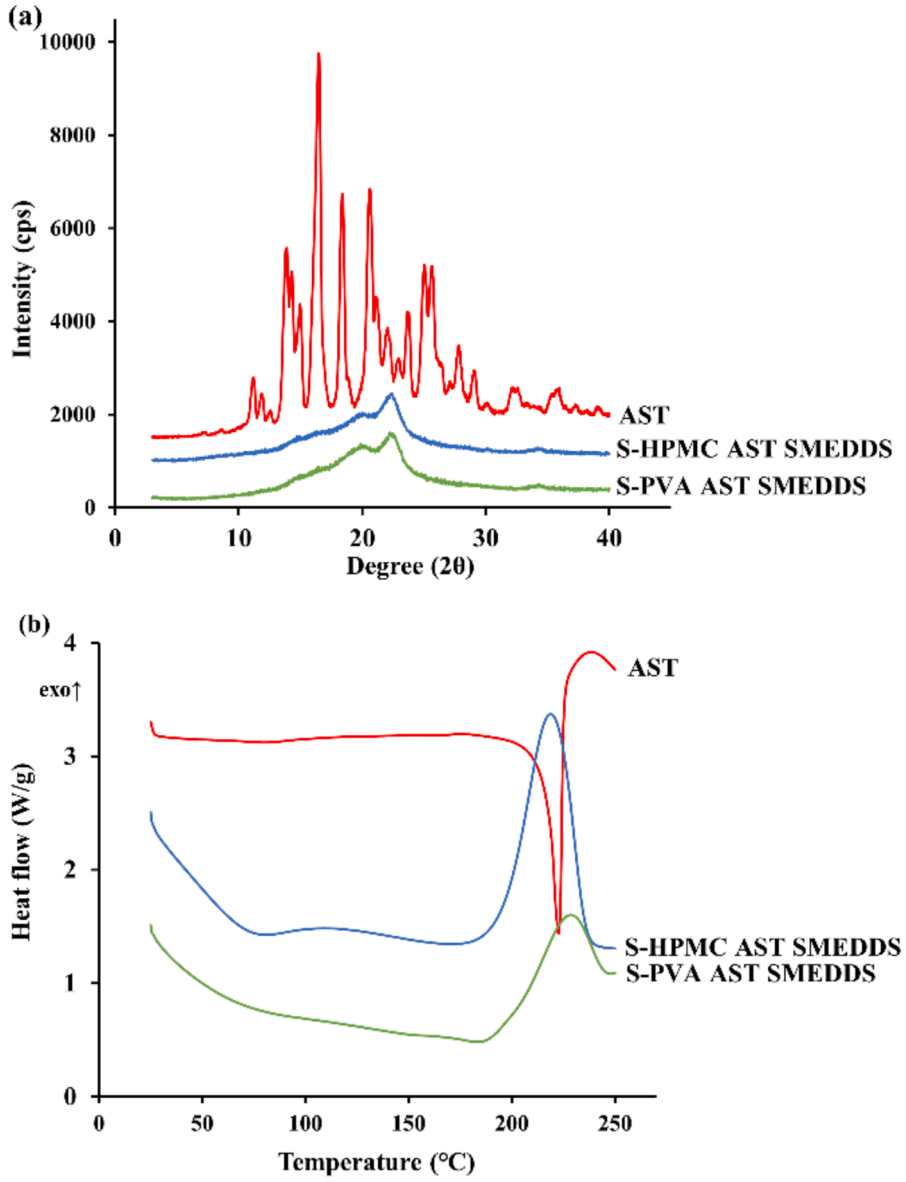

Fig. 2. (a) Powder X-ray diffraction patterns and (b) differential scanning calorimetry thermograms of AST raw material, S-HPMC AST SMEDDS, and S-PVA AST SMEDDS.

number of sharp diffraction peaks of pure AST powder were observed at 2 theta degrees of 11.84, 13.88, 16.48, 18.36, 20.58, 25.4, 25.6, 27.8, 32.28, and 35.36, which confirmed the crystal form of AST (Pan et al., 2018). In PXRD patterns obtained from the spray-dried powders, all major sharp peaks of AST disappeared proving the complete transformation of crystalline AST to the amorphous form in our developed systems using the spray drying method. Meanwhile, including MCC as a solid carrier in both S-AST SMEDDS formulas revealed amorphous appearance with the presence of two broad peaks at 20.54° and 22.36° (2θ) as these peaks were anticipated from the crystal and amorphous nature of MCC originated from spray-dried wood cellulose powders (Nakai et al., 1977). Overall, it was noted that the supersaturable AST SMEDDS was completely adsorbed onto MCC and was dispersed in the polymer (HPMC or PVA) matrix. Additionally, this might be also assumed that our developed SMEDDS system containing PPIs successfully inhibited the nucleation and precipitation of AST and thus maintained the sufficient amounts of AST as the solubilized form (Quan et al., 2017; Sharma et al., 2020). As a consequence, the enhancement of the apparent solubility and the improvement of the dissolution profile of AST should be expected to occur in our formulations.

Changes in thermotropic phase behaviors of pure AST powder, S-HPMC AST SMEDDS, and S-PVA AST SMEDDS were measured by DSC, and the thermograms were displayed in Fig. 2 (b). The sharp endothermic peak of AST was observed at approximately 222 °C which referred to the phase transformation (melting) of AST (Pan et al., 2018). The melting peak of AST completely disappeared in the thermograms of S-HPMC AST SMEDDS and S-PVA AST SMEDDS, but the broad exothermic peaks appeared at around 219 °C in S-HPMC AST SMEDDS and 227 °C in S-PVA AST SMEDDS. These results were in agreement with the data reported by Dalvadi et al. (2017). However, these exothermic peaks were caused by the formulation containing of L-SMEDDS (rice bran oil, Kolliphor® RH 40, and Span® 20) in spray-dried powders because the exothermic peak of the blank S-SMEDDS (without AST) had been confirmed by DCS analysis. Besides, disappearance of the endothermic peak of AST in S-HPMC AST SMEDDS and S-PVA AST SMEDDS DSC thermograms might be due to the interaction of compositions in the SMEDDS formulation. It was also hypothesized that the supersaturated amount of AST uniformly adsorbed into the internal surfaces of the MCC solid carrier and PPI.

3.2. Physicochemical properties of AST SMEDDS tablets

After manufacturing tablets by direct compression, HPMC AST SMEDDS tablets and PVA AST SMEDDS tablet were evaluated for physicochemical properties including size (diameter × thickness), weight, hardness/crushing strength, friability, and AST content as reported in Table 2. Photographs of AST SMEDDS tablets for both formulas were also displayed in Fig. S2 in the Supplementary Material. After reconstitution of tablets in water, the mean droplet sizes of the self-assembling microemulsions obtained from HPMC AST SMEDDS tablets and PVA AST SMEDDS tablets were measured as 181.27 ± 21.56 nm with a PDI of 0.72 ± 0.06 and 212.90 ± 46.71 nm with a PDI of 0.54 ± 0.03, respectively, which were larger than the droplet size of self-microemulsions from L-AST SMEDDS (40.79 ± 3.11 nm with a PDI of 0.25 ± 0.06). Meanwhile, the zeta potential values, −38.53 ± 1.62 for HPMC AST SMEDDS tablet and −41.37 ± 0.64 for PVA AST SMEDDS tablet, were more negative than that from L-AST SMEDDS (-25.83 ± 1.92 mV). A larger droplet size of self-microemulsion from AST SMEDDS tablets than that from L-AST SMEDDS suggested a strong attraction between surfactants and hydrophilic PPIs in the tablets. Not only was a polymer incorporated in many droplets, but it could be also adsorbed on the interfaces of microemulsion droplets which could lead to droplet clusters. Hydrophilic polymers could be adsorbed at the outside interfaces of oil-in-water microemulsions driving the droplet clusters formation (Allgaier and Frielinghaus, 2009). Additionally, more negative values of the zeta potentials of self-microemulsions from AST SMEDDS tablets were caused by PPIs in the tablets owing to the negative charge bearing property of the polymer solutions (Ghadermazi et al., 2019).

3.3. In vitro dissolution of AST SMEDDS tablets

The *in vitro* dissolutions of pure AST powder, L-AST SMEDDS, HPMC AST SMEDDS tablets, and PVA AST SMEDDS tablets were studied in two media of pH 1.2 and pH 6.8 in a sequential manner representing GI fluids as described above in the method section. Displayed in Fig. 3, the *in vitro* release profiles of both HPMC AST SMEDDS tablets and PVA AST SMEDDS tablets depended upon pH of the dissolution medium. Both HPMC AST SMEDDS tablets and PVA AST SMEDDS tablets showed slow release rates in pH 1.2 medium during an initial stage (0 to 120 min) compared to that of L-AST SMEDDS. At the time point of 120 min in pH 1.2 medium, the cumulative releases of AST from HPMC AST SMEDDS tablets and PVA AST SMEDDS tablets were measured as 50.49 ± 1.79% and 42.95 ± 3.07%, respectively, while that from L-AST SMEDDS was more than 90%. These results were in an agreement with previous research done by Yeom et al. (2017) who developed an optimized valsartan loaded Su-SMEDDS tablet with a super-disintegrant (croscarmellose sodium, 6.3% of tablet weight) using a D-optimal mixture design, and they studied *in vitro* dissolution profiles of valsartan loaded tablets, granules, powder, and commercial product in pH 1.2 medium. The release profile of valsartan loaded Su-SMEDDS tablet was comparably slower (< 60%) than that of valsartan loaded granules and liquid SMEDDS. In our study, HPMC AST SMEDDS tablets and PVA AST SMEDDS tablets were prepared with 2% of croscarmellose sodium (CCS) of a total weight of a tablet, and the cumulative releases of AST SMEDDS tablets (≤ 50%) were similar to their findings in pH 1.2 dissolution medium. Moreover, Zhao and Augsburger (Zhao and Augsburger, 2005) evaluated water uptake and swelling rate of CCS which were significantly slower in an acidic medium (0.1 N HCl) because the ionizable carboxylate groups of CCS behaved like a weak acid and could be unionized in an acidic medium leading to the slow swelling rate. According to the previous work (Berardi et al., 2021), CCS was less influenced by ionic strength, ethanol content, and viscosity of the dissolution medium. Regarding the polymers used in HPMC AST SMEDDS tablets and PVA AST SMEDDS tablets, HPMC (non-ionic cellulosic hydrophilic polymer) and PVA (biocompatible synthetic hydrophilic polymer) could be soluble in both pH media (Józó et al., 2022). Therefore, the results suggested that a disintegrant (CCS) considerably affected the release profiles of the developed AST SMEDDS tablets depending on the changes in pH medium.

Meanwhile, in the later stage the dissolution rates of both tablets in pH 6.8 were noticeably increased between 120 and 480 min and maintained at 99.47 ± 0.22% for HPMC AST SMEDDS tablets and 98.52 ± 0.99% for PVA AST SMEDDS tablets at the end of 480 min. Although

Table 2
Some physicochemical properties of AST SMEDDS tablets for the two formulations (HPMC AST SMEDDS tablet and PVA AST SMEDDS tablet) containing different types of polymers. Results were expressed as mean ± standard deviation (SD) of the tablet samples. Sample numbers $n = 6$ for diameter, thickness, and hardness, and $n = 10$ for weight, friability, and AST content measurements.

AST SMEDDS tablets	Diameter (mm)	Thickness (mm)	Weight (g)	Hardness (N)	Friability (%)	AST content (%)
HPMC AST SMEDDS tablets	20.22 ± 0.01	2.89 ± 0.01	1.002 ± 0.002	64.72 ± 1.64	0.49	102.22 ± 0.76
PVA AST SMEDDS tablets	20.22 ± 0.01	2.88 ± 0.02	1.003 ± 0.001	64.89 ± 1.15	0.64	100.42 ± 0.75

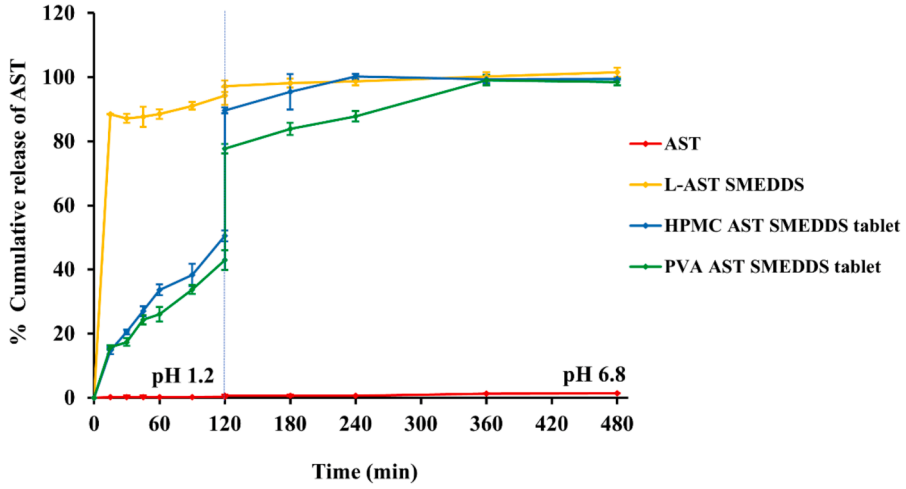

Fig. 3. *In vitro* dissolution profiles of AST raw material, L-AST SMEDDS, HPMC AST SMEDDS tablet, and PVA AST SMEDDS tablet in pH 1.2 and 6.8 media.

the release profiles of HPMC AST SMEDDS tablets and PVA AST SMEDDS tablets were quite similar in both dissolution media, the HPMC-incorporated AST SMEDDS tablet release rate was slightly faster than that of PVA-containing AST SMEDDS tablet especially during 120−360 min. Bianchi et al. (2011) evaluated the modified release effect of and the contribution from HPMC:PVA blends in two types of pH media (pH 1.2 hydrochloric acid buffer and pH 6.0 phosphate buffer) and found that PVA controlled the drug dissolution rate providing the modified release profile and that HPMC was totally solubilized in both pH media. It was important to point out that an appropriate polymer should be chosen to control the rate and extent of AST released from the tablets. For L-AST SMEDDS, the fastest dissolution profile was observed with 88.47 ± 0.10% of the total AST content released within 15 min in pH 1.2 medium and maintained at 101.06 ± 1.44% in pH 6.8 after reaching the plateau until 480 min. These data pointed out that rapid self-assembling of microemulsions from L-SMEDDS would enhance the dissolution of AST. In contrast, solubility of AST raw material powder in both media was quite extremely low (<1.5%) until the end of dissolution study. Overall, dissolution profiles of the developed AST SMEDDS tablets were satisfactorily improved comparable to L-AST SMEDDS supporting an enhancement of oral bioavailability by successfully incorporating lipophilic compound AST and hydrophilic polymers in the SMEDDS carrier system.

3.4. *In vitro* cellular antioxidant activity of AST SMEDDS tablets

In vitro free radical scavenging activity by a DPPH assay and Caco-2 cell viability testing by an MTT assay of the AST SMEDDS formulations were essentially performed before the subsequent experiments. The DPPH radical scavenging activities of the AST SMEDDS formulations were measured and shown in Fig. S3 in the Supplementary Material which supported the results on cellular antioxidant activities in this section. Additionally, the impact of the AST SMEDDS formulations on viability of Caco-2 cells was investigated by the MTT assay in order to conduct further cellular experiments, and it was displayed in Fig. S4 in the Supplementary Material file.

Cellular antioxidant activity was measured by using a $DCFH_2$-DA spectrofluorometric assay. $DCFH_2$-DA (non-polar) diffuses through the cells and is deacetylated by a cellular esterase enzyme to $DCFH_2$ which is oxidized to fluorescence DCF (polar) in the presence of peroxyl radical (ROO•) (Wan et al., 2015). Therefore, the degree of oxidation is reflected by the level of DCF fluorescence. Reactive oxygen species (ROS) are highly unstable and quickly react with molecules to get an electron resulting in excessive accumulation of ROS within the cells which can cause oxidative stress-related diseases. AST can directly or indirectly inhibit oxidation by reducing the production of ROS (Yang et al., 2013; Zuluaga et al., 2017). Owing to the unique structure of AST having a polar-nonpolar-polar skeleton, it can quench the free radicals inside and outside of the phospholipid bilayers. Thereby, AST disturbs the oxidative chain reactions of free radicals such as ROS (Dai et al., 2020).

For examination on suppression of the oxidation process, we investigated ROS generation in the Caco-2 cells. Displayed in Fig. 4, at the dilution of 1:250, pure AST powder showed over 93% DCF level indicating a relatively low ROS scavenging efficiency while DCF levels in L-AST SMEDDS, HPMC AST SMEDDS tablets, and PVA AST SMEDDS tablets treated cells were 36%, 53%, and 58%, respectively, demonstrating greater ROS scavenging efficiency than AST raw material. A similar trend was also observed in the other dilutions (1:500 and 1:1000) of the samples. Moreover, ROS eliminations were not significantly different between HPMC AST SMEDDS tablet and PVA AST SMEDDS tablets at the 1:250 ratio. The ROS scavenging efficiency was dependent on the concentration of the compound having an antioxidant activity (Haung et al., 2020) and the carrier system to permeate through the cells (Nalawade and Gajjar, 2015), especially for HPMC AST SMEDDS tablets and PVA AST SMEDDS tablets that the DCF levels trended to decrease with an increase in the sample concentrations. Nonetheless, the cellular antioxidant activity of L-AST SMEDDS was nearly the same in all dilution ratios. In general, AST molecule was likely to accumulate in the cell membranes and protected the cells from peroxidation (Fujii et al., 2015). However, the intracellular AST concentration was low due to the hydrophilic nature of the cytoplasm. Therefore, hydrophilic polymers and oil in water (o/w) microemulsions were usually included in the AST delivery system for ease of internalization and accumulation of AST in the cytoplasm of the cells (Nalawade and Gajjar, 2015). As a consequence, the intracellular oxidative chain reaction was more easily terminated by self-assembling microemulsions from the AST SMEDDS formulations compared to pure AST powder. This study suggested that AST SMEDDS based formulations successfully inhibited the intrinsic ROS production.

3.5. Cellular uptake of coumarin 6-labeled SMEDDS tablets

The fluorescence microscope was used to visually observe an uptake nature of SMEDDS in the cells. Although some other work showed that a fluorescence microscope could detect AST biosynthesized in the yeast or algae cells at some wavelength, according to our preliminary results AST absorbed in the Caco-2 cells could not be measured by a fluorescence microplate reader. In this research, a fluorescence dye coumarin 6 (C6) was therefore utilized as an imitator of lipophilic AST for the cellular uptake analysis. C6 was stable in SMEDDS formulations after

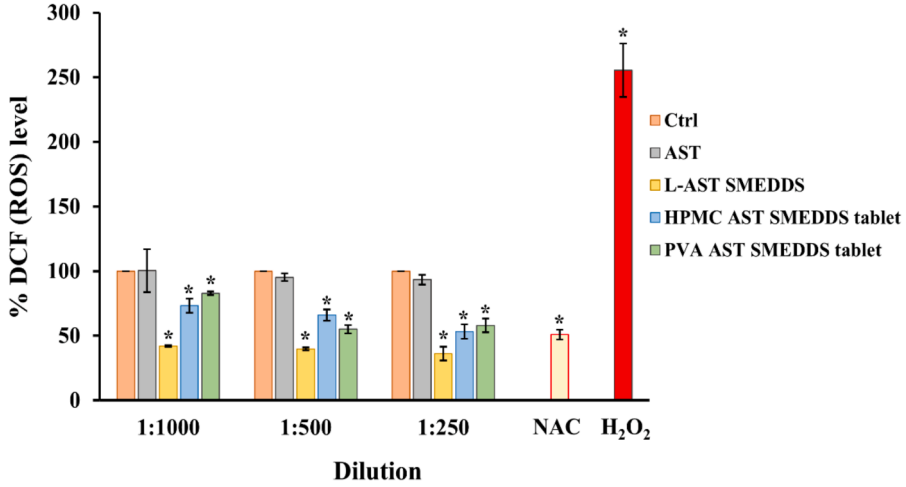

Fig. 4. Effect of formulations containing AST (AST raw material, L-AST SMEDDS, HPMC AST SMEDDS tablet, and PVA AST SMEDDS tablet) on ROS production in Caco-2 cells by quantitative analysis of DCFH-DA after 24-h incubation. * $p < 0.05$ compared to control (Ctrl), $n = 3$. ROS refers to as reactive oxygen species. 5 mM N-acetyl cystine (NAC) is used as a positive control, and 100 mM H_2O_2 is a negative control.

encapsulation. Moreover, after internalization within the cells, C6 did not induce acute toxicity to the cells and it could stay within the cells without immediate release out of the cells (Ibrahim and Rosli, 2020). Hoechst33342 was used for staining nuclei of Caco-2 cells. The blue stains indicated nuclei, and the green fluorescence represented C6 uptakes in the cell cytoplasm. Cellular uptake of all formulations showed the time-dependent manner, and fine localization of C6 was observed inside the cytoplasm of Caco-2 cells as shown in Fig. 5(a). Low intensity of green fluorescence for C6 powder indicated poor uptake of C6 by the cells whereas higher intensities were obtained in L-C6 SMEDDS, HPMC C6 SMEDDS tablets, and PVA C6 SMEDDS tablets. The enhancement of C6 uptake by cells could be owing to the microemulsion droplets and the presence of surfactants such as Kolliphor® RH 40 and Span® 20 (Shen et al., 2019). This indicated that microemulsions assembled from the SMEDDS formulations could increase the dissolved amount of the lipophilic active ingredient and thereby enhance the cellular uptake.

Based on our study, C6 fluorescence intensities in the cells were further analyzed by a fluorescence microplate reader. Displayed in Fig. 5 (b), the fluorescence intensities of C6 and L-C6 SMEDDS were significantly lower than those of HPMC C6 SMEDDS tablets and PVA C6 SMEDDS tablets after 1 h of incubation. However, after 2-h and 4-h treatments, the intensities of C6 powder were noticeably lower than those of L-C6 SMEDDS, HPMC C6 SMEDDS tablets, and PVA C6 SMEDDS tablets. The intensities of L-C6 SMEDDS, HPMC C6 SMEDDS tablets, and PVA C6 SMEDDS tablets were nearly identical at the 2-h measurement whereas intensities of L-C6 SMEDDS and PVA C6 SMEDDS tablets were not significantly different after 4-h incubation but were substantially lower than that of HPMC C6 SMEDDS tablets. In general, the time-dependent behavior was most noticeable in C6 and HPMC C6 SMEDDS tablets whereas the intensity of HPMC C6 SMEDDS tablets was significantly greater than other formulations after 4 h of treatment. This could be due to the effect of HPMC in HPMC C6 SMEDDS tablets which promoted not only mucoadhesive properties but also a synergistic effect on surfactant penetration (Liu et al., 2019).

The next experiment was performed by flow cytometry which was based on the principle of forward-scattered light (cell size) and C6 fluorescence intensities to confirm cellular uptake, and the results were shown in Fig. 6. In this study, background fluorescence of the untreated cells (horizontal *y*-axis value <1000) was excluded for counting. After 4 h of a predetermined treatment, the intracellular C6 uptake was significantly highest in HPMC C6 SMEDDS tablets (above 90%) while those of L-C6 SMEDDS and PVA C6 SMEDDS tablets were nearly 70% and 74%, respectively (Fig. 6 (a)). An increase in cellular uptake of carotenoids in emulsions was considered to be caused by two factors: emulsion droplet size and emulsifier type (Lu et al., 2016). These results were consistent with the data obtained from the fluorescence microplate reader. The red dot plots of control (unstained), C6 powder, L-C6 SMEDDS, HPMC C6 SMEDDS tablet, and PVA C6 SMEDDS tablet were shown in Fig. 6 (b). Low and high areas indicated with red rectangles in the corresponding left and right upper corners of the diagram for C6 intensity were defined based on the gathering Caco-2 cell population of the control (unstained) group. Among C6-labeled formulations, the majority of the cell population treated with HPMC C6 SMEDDS tablet accumulated in high intensity area of C6 fluorescence. Meanwhile, nearly one-third of cell populations in L-C6 SMEDDS and PVA C6 SMEDDS tablet samples located in low intensity areas, and their cellular uptakes were lower than that of HPMC C6 SMEDDS tablet. Regarding C6 powder, half of the cell population still showed C6 uptake which might be due to the effect of DMSO used as a solvent for analyzing the cellular activities of carotenoids (Yang et al., 2017). In this work, on the basis of the same emulsifiers used in the SMEDDS formulas, the smaller self-microemulsion droplets obtained from HPMC C6 SMEDDS tablet were, the greater uptake would be achieved (Shen et al., 2019). However, cellular uptakes of both liquid (L) and solid (HPMC C6 SMEDDS tablet and PVA C6 SMEDDS tablet) SMEDDS formulations were significantly higher than that of C6 pure powder indicating the enhanced cellular uptake of C6 via SMEDDS. This study confirmed that SMEDDS played a major role in the cellular uptake mechanism via internalizing the active compound into the cell cytoplasm.

3.6. Cellular uptake of AST from SMEDDS tablets

After Caco-2 cellular uptake had been studied by using C6 fluorescence dye in formulations instead of AST, cellular uptake of AST in the samples was further examined to confirm the uptake efficiency of AST from SMEDDS tablets in Caco-2 cells. As depicted in Fig. 7, all AST-loaded formulations showed significantly higher cellular uptake efficiency than AST raw material, which indicated an enhanced enterocyte cellular uptake of AST via SMEDDS. However, the difference in the uptake amount between AST and C6 in the cells might be due to the physicochemical properties of the measured substance (such as structural configuration, molecular weight, log *P* value, cell membrane permeability) and cellular uptake measurement conditions. After incubation for 4 h, the percentage of intracellular uptake of AST powder, L-AST SMEDDS, HPMC AST SMEDDS tablet, and PVA AST SMEDDS tablet was 25.88 ± 0.05, 70.95 ± 7.53, 37.76 ± 0.04, and 36.89 ± 0.06,

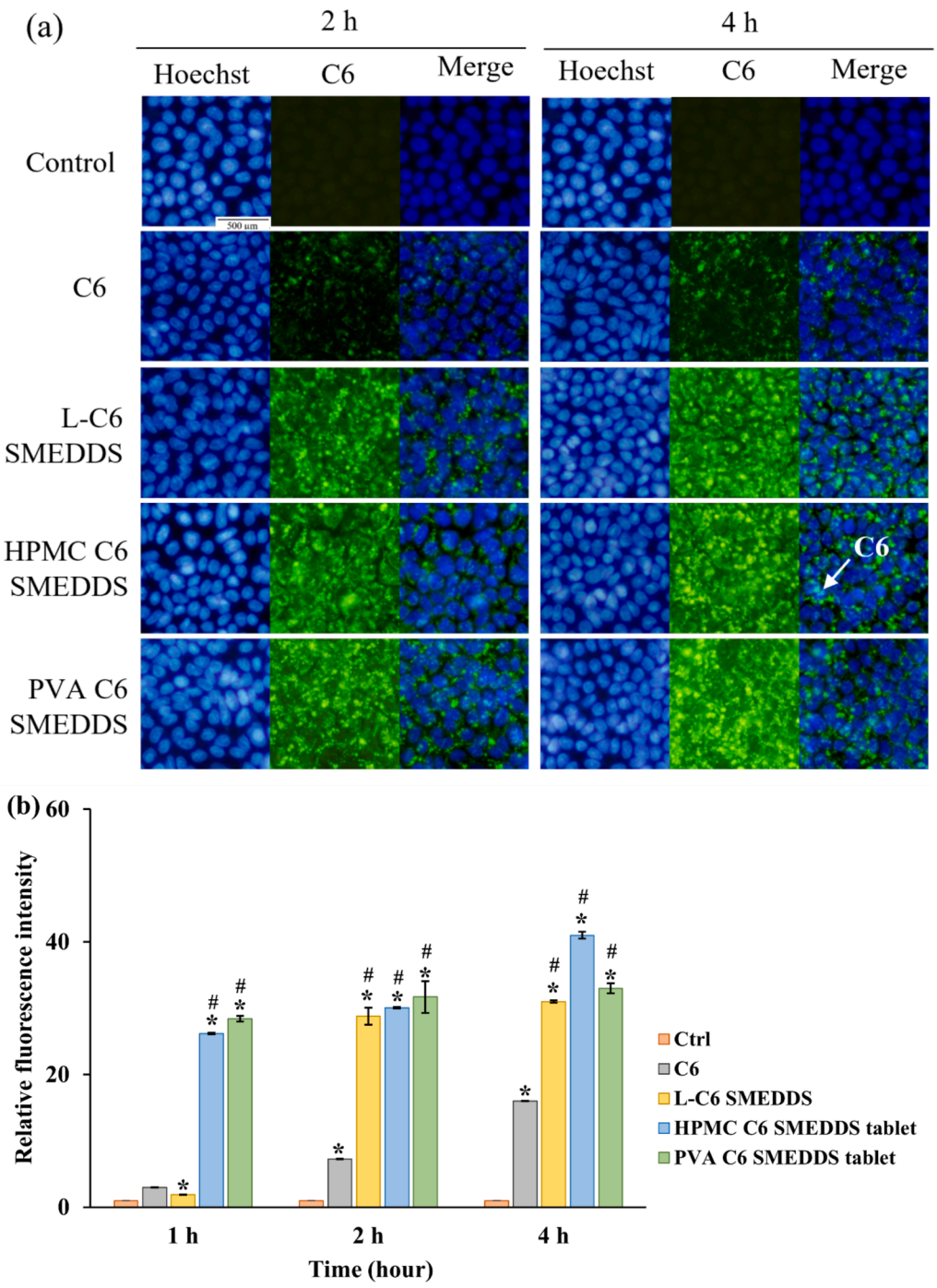

Fig. 5. Cellular distribution of coumarin 6 (C6)-loaded samples including C6 powder, L-C6 SMEDDS, HPMC C6 SMEDDS tablet, and PVA AST SMEDDS tablet in Caco-2 cells: (a) Fluorescence microscope images of Caco-2 cells after 2-h and 4-h treatment with samples and stained with Hoechst (blue fluorescence, nuclei); (b) Relative fluorescence intensity in the cells measured by a multipurpose fluorescence microplate reader for different time intervals. * $p < 0.05$ versus control (Ctrl) and $^{\#}$ $p < 0.05$ versus C6 powder, $n = 3$.

respectively. Among these formulations, the greatest AST cellular uptake was seen in L-AST SMEDDS whereas AST cellular uptakes from HPMC AST SMEDDS tablet and PVA AST SMEDDS tablet were nearly half of the uptake from L-AST SMEDDS formulation. It was also observed that there was insignificant difference in AST cellular uptake efficiency for the two (HPMC versus PVA) AST SMEDDS tablet formulas. It was noted that L-AST SMEDDS producing smaller self-microemulsion droplet size could penetrate the cell membrane in higher extent compared to the AST SMEDDS tablets. Our result was supported by the previous work reporting that small droplet size of emulsion (< 200 nm) easily passed through the epithelial cells via passive transport (Haung et al., 2020). Convincingly, it could be inferred that the AST-loaded SMEDDS formulations could improve cellular uptake of AST into Caco-2 cells and lead to an enhanced oral bioavailability of AST.

3.7. Stability profiles of AST SMEDDS tablets

AST can gradually degrade during storage because the polyunsaturated skeleton of AST molecule is susceptible to heat, light, and oxygen concentration. For assessing the thermal stabilities of AST SMEDDS tablets under specified storage conditions for 3 months, HPMC AST SMEDDS tablets and PVA AST SMEDDS tablets were tested on some physicochemical properties including hardness, friability, and moisture content after each storage time period. It was observed that both HPMC AST SMEDDS tablets and PVA AST SMEDDS tablets showed no significant changes in their physicochemical properties up to three months.

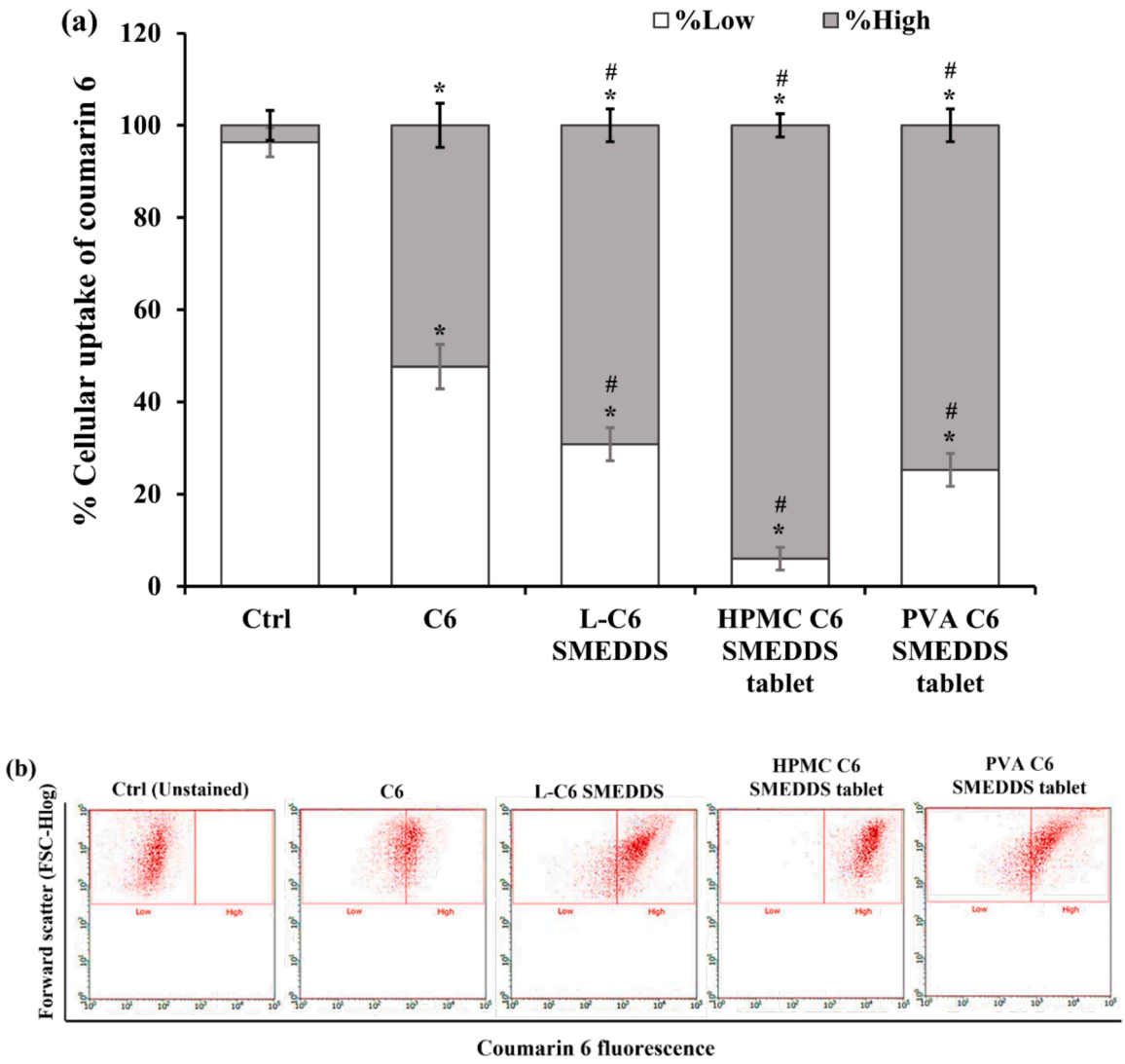

Fig. 6. Cellular uptake of coumarin 6 (C6)-loaded samples including C6 powder, L-C6 SMEDDS, HPMC C6 SMEDDS tablet, and PVA C6 SMEDDS tablet in Caco-2 cells after 4-h incubation: (a) percentage of cellular uptake (%); (b) flow cytometric analysis diagrams. All data (mean ± SD) were performed in triplicates. * $p < 0.05$ versus control (Ctrl) and # $p < 0.05$ versus C6 powder.

After reconstitution of AST SMEDDS tablets stored under these two conditions, droplet size, PDI, and zeta potential of the self-assembling microemulsions formed from HPMC AST SMEDDS tablets and PVA AST SMEDDS tablets were evaluated (see Table 3). For the HPMC ASTSMEDDS tablets stored at 30 ± 2 °C/ RH 65 ± 5%, the properties insignificantly changed up to three months compared to its initial values. For the PVA AST SMEDDS tablets kept at 30 ± 2 °C/ RH 65 ± 5%, the droplet size of its self-microemulsion did not change significantly. However, the droplet sizes of microemulsions from both HPMC AST SMEDDS tablets and PVA AST SMEDDS tablets drastically increased at 40 ± 2 °C/ RH 75 ± 5%. PDI and zeta potential values from the PVA AST SMEDDS tablet slightly varied at both storage conditions.

The contents (%) of the active compound in AST SMEDDS tablets were determined during 3-month storage and shown in Table 3. AST contents in both HPMC AST SMEDDS tablets and PVA AST SMEDDS tablets slowly decreased upon the storage time and with an increased temperature. Pu et al. (2011) reported that the degradation rate of AST in microencapsulated powder prepared by a spray drying technique was faster at higher storage temperature than that at low storage temperature. At the end of three months, at 30 °C, AST remaining (%) in HPMC AST SMEDDS tablets was 93.83 ± 1.14% and in PVA AST SMEDDS tablet was 94.58 ± 0.40% while AST contents in HPMC AST SMEDDS tablets and PVA AST SMEDDS tablets were significantly decreased to 83.27 ± 0.32% and 84.58 ± 0.37%, respectively, at 40 °C. These results agreed with the findings of Affandi et al. (2011) that AST loaded nanoemulsion had higher degradation rate at 40 ± 2 °C/ RH 75 ± 5% in a 90-day stability study. This was due to the heat-sensitive nature of AST after exposed to a high temperature for a long period of time. Comparing between HPMC- and PVA-incorporated tablets, AST contents in PVA AST SMEDDS tablets containing PVA were slightly greater than those in HPMC AST SMEDDS tablets containing HPMC at both storage conditions. However, the differences in AST content between HPMC AST SMEDDS tablets and PVA AST SMEDDS tablets were not statistically significant at low and high temperatures after three-month storage. Overall, the self-microemulsion properties and AST content were not considerably affected by low temperature (30 °C) and low humidity (65% RH). For these reasons, it can be suggested that AST SMEDDS tablets should be kept at 30 ± 2 °C/ RH 65 ± 5%.

4. Conclusions

To summarize, AST SMEDDS tablets were successfully designed and evaluated for an enhancement of the dissolution, antioxidant activity, intestinal Caco-2 cell uptake, and absorption. The attempt had been

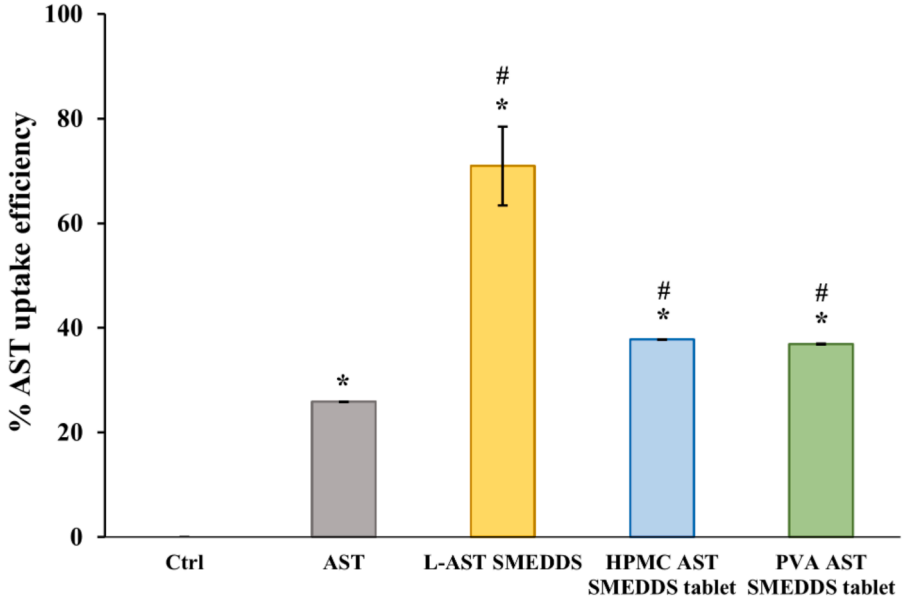

Fig. 7. Cellular uptake efficiency (%) of AST-loaded samples including AST raw material, L-AST SMEDDS, HPMC AST SMEDDS tablet, and PVA AST SMEDDS tablet in Caco-2 cells after 4-h incubation. All data (mean ± SD) were performed in triplicates. * $p < 0.05$ versus control (Ctrl) and # $p < 0.05$ versus AST powder.

Table 3
Stability profiles of HPMC AST SMEDDS tablets and PVA AST SMEDDS tablets stored at two different temperatures and relative humidity (RH) percentages within 3 months. Droplet size (nm), polydispersity index (PDI), zeta potential (mV), and AST content (%) of the self-assembling microemulsions reconstituted from AST SMEDDS tablets ($n = 3$) were measured. Results were expressed as mean ± standard deviation (SD).

Month	30 ± 2 °C/ RH 65 ± 5%		40 ± 2 °C/ RH 75 ± 5%	
	HPMC AST SMEDDS tablets	PVA AST SMEDDS tablets	HPMC AST SMEDDS tablets	PVA AST SMEDDS tablets
	Droplet size (nm)			
0	181.27 ± 21.56	212.90 ± 46.71	181.27 ± 21.57	212.90 ± 46.71
1	198.03 ± 38.49	206.87 ± 18.88	244.73 ± 42.31	313.70 ± 39.57
2	191.99 ± 6.90	233.22 ± 11.89	247.17 ± 22.05	321.38 ± 11.87
3	206.69 ± 23.72	243.01 ± 17.30	246.37 ± 10.73	327.39 ± 12.25
	PDI			
0	0.72 ± 0.06	0.54 ± 0.03	0.72 ± 0.06	0.54 ± 0.03
1	0.64 ± 0.10	0.67 ± 0.05	0.64 ± 0.01	0.57 ± 0.03
2	0.69 ± 0.03	0.64 ± 0.04	0.65 ± 0.03	0.64 ± 0.05
3	0.65 ± 0.08	0.67 ± 0.02	0.67 ± 0.04	0.61 ± 0.04
	Zeta potential (mV)			
0	-38.53 ± 1.62	-41.37 ± 0.64	-38.53 ± 1.62	-41.37 ± 0.64
1	-37.93 ± 1.01	-45.77 ± 2.32	-38.73 ± 1.61	-48.80 ± 1.95
2	-37.85 ± 4.92	-38.52 ± 2.99	-37.34 ± 1.10	-46.30 ± 0.70
3	-32.59 ± 4.27	-46.98 ± 0.59	-34.18 ± 1.63	-43.31 ± 2.69
	AST content (%)			
0	102.22 ± 0.76	100.42 ± 0.75	102.22 ± 0.76	100.42 ± 0.75
1	98.47 ± 0.99	98.31 ± 0.27	90.89 ± 0.47	89.13 ± 0.42
2	96.02 ± 0.17	97.25 ± 0.18	88.42 ± 0.59	90.28 ± 0.64
3	93.83 ± 1.14	94.58 ± 0.40	83.27 ± 0.32	84.58 ± 0.37

made to prepare AST SMEDDS spray-dried powders by mixing L-AST SMEDDS (rice bran oil, Kolliphor® RH 40, and Span® 20) with a solid carrier (MCC) and hydrophilic polymers (HPMC and PVA) prior to compression into tablets. Solid state characterization on S-AST SMEDDS confirmed that AST was changed into the molecular disperse in a dissolved state showing compatibility with other excipients. The microemulsion droplet size was approximately 200 nm with a high zeta potential value (approximately −40 mV) after reconstitution of tablets, which can provide greater surface area to increase dissolution profiles of AST. To maximize the absorption in GI tract, HPMC and PVA were used as precipitation inhibitors. Having polymers, SMEDDS tablets exhibited higher concentrations and better dissolution profiles of AST in both simulated gastric fluid and simulated intestinal fluid than AST bulk powder. Our results in Caco-2 cell line clearly demonstrated that AST SMEDDS tablets decreased ROS generation and increased intestinal cellular uptake and absorption. Additionally, our developed AST SMEDDS tablets were chemically and physically stable at 30 ± 2 °C/ RH 65 ± 5% in a 3-month stability study. Our research suggested that AST SMEDDS tablets could be a promising platform for improving AST permeation, absorption, and thus oral bioavailability. Other types of hydrophilic polymers and other excipients incorporated in the AST SMEDDS tablets could be further studied to investigate their effects on dissolution profiles, antioxidant activities, and cellular uptake. Future studies should be conducted *in vivo* including preclinical studies in animal models to obtain pharmacokinetic data of the AST SMEDDS tablets as well as clinical studies in human subjects to further prove safety and efficacy of the newly developed AST SMEDDS tablet dosage form.

CRediT authorship contribution statement

Wai Thet Aung: Conceptualization, Methodology, Investigation, Data curation, Formal analysis, Visualization, Validation, Resources, Writing – original draft, Writing – review & editing. **Hnin Ei Ei Khine:** Investigation, Formal analysis, Visualization, Validation, Writing – review & editing. **Chatchai Chaotham:** Methodology, Investigation, Formal analysis, Visualization, Validation, Writing – review & editing, Supervision. **Veerakiet Boonkanokwong:** Conceptualization, Methodology, Investigation, Data curation, Formal analysis, Visualization, Validation, Resources, Writing – original draft, Writing – review & editing, Supervision, Project administration, Funding acquisition.

Declaration of Competing Interest

The authors declare no conflicts of interest. The authors alone are responsible for the content and writing of this article.

Acknowledgments

One of the authors (Ms. W.T. Aung) acknowledged the Scholarship Program for ASEAN Countries granted from the Office of Academic Affairs, Chulalongkorn University for a financial support during her doctoral degree study. This research was supported by the Graduate Program of Pharmaceutical Sciences and Technology, Faculty of Pharmaceutical Sciences and the Graduate School Thesis Grant, Chulalongkorn University (Grant ID: GCUGR1225643034D No. 034). The authors gratefully appreciated the Grants for Development of New Faculty Staff, Ratchadaphiseksomphot Endowment Fund, Chulalongkorn University (Grant ID: DNS 62_008_33_001_1). This work was also partially funded by the Agricultural Research Development Agency (Public Organization) of Thailand. The researchers would like to thank Professor Dr. Garnpimol C. Ritthidej for being a mentor and guiding this project. The authors also want to thank the Pharmaceutical Research Instrument Center and Chulalongkorn University Drug and Health Products Innovation Promotion Center (CU-D-HIP) of the Faculty of Pharmaceutical Sciences, and the Scientific and Technological Research Equipment Centre of Chulalongkorn University for providing research instruments.

Supplementary materials

Supplementary material associated with this article can be found, in the online version, at doi:10.1016/j.ejps.2022.106263.

References

Affandi, M.M.M., Julianto, T., Majeed, A., 2011. Development and stability evaluation of astaxanthin nanoemulsion. Asian J. Pharm. Clin. Res. 4, 142–148.

Al-Zoubi, N., Gharaibeh, S., Aljaberi, A., Nikolakakis, I., 2021. Spray drying for direct compression of pharmaceuticals. Processes 9, 267. https://doi.org/10.3390/pr9020267.

Allgaier, J., Frielinghaus, H., 2009. Effects of Polymers on the Properties of Microemulsions. Blackwell Publishing Ltd.

Aung, W.T., Boonkanokwong, V., 2021. Preparation, optimization using a mixture design, and characterization of a novel astaxanthin-loaded rice bran oil self-microemulsifying delivery system formulation. J. Dispers. Sci. Technol. 1–14. https://doi.org/10.1080/01932691.2021.2016436.

Aung, W.T., Boonkanokwong, V., 2022. Impact of polymers as precipitation inhibitors on physicochemical properties of spray-dried astaxanthin-loaded self-microemulsifying delivery systems. Key Eng. Mater. 914, 15–21.

Badria, F.A., Fayed, H.A., Ibraheem, A.K., State, A.F., Mazyed, E.A., 2020. Formulation of sodium valproate nanospanlastics as a promising approach for drug repurposing in the treatment of androgenic alopecia. Pharmaceutics 12. https://doi.org/10.3390/pharmaceutics12090866.

Berardi, A., Bisharat, L., Quodbach, J., Abdel Rahim, S., Perinelli, D.R., Cespi, M., 2021. Advancing the understanding of the tablet disintegration phenomenon – an update on recent studies. Int. J. Pharm. 598, 120390 https://doi.org/10.1016/j.ijpharm.2021.120390.

Bi, X., Liu, X., Di, L., Zu, Q., 2016. Improved oral bioavailability using a solid self-microemulsifying drug delivery system containing a multicomponent mixture extracted from salvia miltiorrhiza. Molecules 21. https://doi.org/10.3390/molecules21040456.

Bianchi, S.E., Angeli, V.W., Souza, K.C.B.d., Miron, D.d.S., Carvalho, G.d.A., Santos, V.d., Brandalise, R.N., 2011. Evaluation of the solubility of the HPMC: PVA blends in biological fluids in vitro. Mater. Res. 14, 166–171. https://doi.org/10.1590/S1516-14392011005000033.

Capelli, B., Talbott, S., Ding, L., 2019. Astaxanthin sources: Suitability for human health and nutrition. Funct. Food Health Dis. 9, 430–445. https://doi.org/10.31989/ffhd.v9i6.584.

Dai, M., Li, C., Yang, Z., Sui, Z., Li, J., Dong, P., Liang, X., 2020. The astaxanthin aggregation pattern greatly influences its antioxidant activity: a comparative study in Caco-2 cells. Antioxidants 9. https://doi.org/10.3390/antiox9020126.

Dalvadi, H., Patel, N., Parmar, K., 2017. Systematic development of DoE optimized self-microemulsifying drug delivery system of zotepine. J. Microencapsul. 34, 1–31. https://doi.org/10.1080/02652048.2017.1324920.

Fujii, R., Yamano, N., Hashimoto, H., Misawa, N., Ifuku, K., 2015. Photoprotection vs photoinhibition of photosystem II in transplastomic lettuce (Lactuca sativa) dominantly accumulating astaxanthin. Plant. Cell Physiol. 57 https://doi.org/10.1093/pcp/pcv187.

Ghadermazi, R., Hamdipour, S., Sadeghi, K., Ghadermazi, R., Khosrowshahi Asl, A., 2019. Effect of various additives on the properties of the films and coatings derived from hydroxypropyl methylcellulose—a review. Food Sci. Nutr. 7, 3363–3377. https://doi.org/10.1002/fsn3.1206.

Grimmig, B., Kim, S.-H., Nash, K., Bickford, P.C., Douglas Shytle, R., 2017. Neuroprotective mechanisms of astaxanthin: a potential therapeutic role in preserving cognitive function in age and neurodegeneration. Geroscience 39, 19–32. https://doi.org/10.1007/s11357-017-9958-x.

Haung, H.-Y., Wang, Y.-C., Cheng, Y.-C., Kang, W., Hu, S.-H., Liu, D., Xiao, C., Wang, H.-M.D., 2020. A novel oral astaxanthin nanoemulsion from haematococcus pluvialis induces apoptosis in lung metastatic melanoma. Oxid. Med. Cell. Longev. 2020, 2647670 https://doi.org/10.1155/2020/2647670.

Hu, F., Liu, W., Yan, L., Kong, F., Wei, K., 2019. Optimization and characterization of poly(lactic-co-glycolic acid) nanoparticles loaded with astaxanthin and evaluation of anti-photodamage effect in vitro. R. Soc. Open Sci. 6 https://doi.org/10.1098/rsos.191184.

Ibrahim, W.N., Rosli, L.M.B.M., 2020. Formulation, cellular uptake and cytotoxicity of thymoquinone-loaded PLGA nanoparticles in malignant melanoma cancer cells. Int. J. Nanomed. 15, 8059. https://doi.org/10.2147/IJN.S269340.

ICH, 2003. Q1A (R2) Stability testing of new drug substances and products. In: International Conference on Harmonization (ICH), pp. 1–24.

Irnawati, I., Riyanto, S., Martono, S., Rohman, A., 2019. Determination of sesame oil, rice bran oil and pumpkin seed oil in ternary mixtures using FTIR spectroscopy and multivariate calibrations. Food Res. 4, 135–142. https://doi.org/10.26656/fr.2017.4(1).260.

Joshi, G., Kumar, A., Sawant, K., 2016. Bioavailability enhancement, Caco-2 cells uptake and intestinal transport of orally administered lopinavir-loaded PLGA nanoparticles. Drug Deliv. 23, 3492–3504. https://doi.org/10.1080/10717544.2016.1199605.

Józó, M., Simon, N., Yi, L., Móczó, J., Pukánszky, B., 2022. Improved release of a drug with poor water solubility by using electrospun water-soluble polymers as carriers. Pharmaceutics 14. https://doi.org/10.3390/pharmaceutics14010034.

Kim, M.-S., Ha, E.-S., Choo, G.-H., Baek, I.-H., 2015. Preparation and in vivo evaluation of a dutasteride-loaded solid-supersaturatable self-microemulsifying drug delivery system. Int. J. Mol. Sci. 16, 10821–10833. https://doi.org/10.3390/ijms160510821.

Liu, D., Wu, Q., Chen, W., Lin, H., Zhu, Y., Liu, Y., Liang, H., Zhu, F., 2019. A novel FK506 loaded nanomicelles consisting of amino-terminated poly(ethylene glycol)-block-poly(D,L)-lactic acid and hydroxypropyl methylcellulose for ocular drug delivery. Int. J. Pharm. 562, 1–10. https://doi.org/10.1016/j.ijpharm.2019.03.022.

Lu, W., Kelly, A.L., Maguire, P., Zhang, H., Stanton, C., Miao, S., 2016. Correlation of emulsion structure with cellular uptake behavior of encapsulated bioactive nutrients: influence of droplet size and interfacial structure. J. Agric. Food Chem. 64, 8659–8666. https://doi.org/10.1021/acs.jafc.6b04136.

Mandić, J., Pirnat, V., Luštrik, M., German Ilić, I., Vrečer, F., Gašperlin, M., Zvonar Pobirk, A., 2020. Solidification of SMEDDS by fluid bed granulation and manufacturing of fast drug release tablets. Int. J. Pharm. 583, 119377 https://doi.org/10.1016/j.ijpharm.2020.119377.

Mandić, J., Zvonar Pobirk, A., Vrečer, F., Gašperlin, M., 2017. Overview of solidification techniques for self-emulsifying drug delivery systems from industrial perspective. Int. J. Pharm. 533, 335–345. https://doi.org/10.1016/j.ijpharm.2017.05.036.

Mao, X., Sun, R., Tian, Y., Wang, D., Ma, Y., Wang, Q., Huang, J., Xia, Q., 2019. Development of a solid self-emulsification delivery system for the oral delivery of astaxanthin. Eur. J. Lipid Sci. Technol. 121, 1–10. https://doi.org/10.1002/ejlt.201800258.

Martínez-Delgado, A.A., Khandual, S., Villanueva–Rodríguez, S.J., 2017. Chemical stability of astaxanthin integrated into a food matrix: effects of food processing and methods for preservation. Food Chem. 225, 23–30. https://doi.org/10.1016/j.foodchem.2016.11.092.

Nakai, Y., Fukuoka, E., Nakajima, S., Hasegawa, J., 1977. Crystallinity and physical characteristics of microcrystalline cellulose. Chem. Pharm. Bull. 25, 96–101. https://doi.org/10.1248/cpb.25.96.

Nalawade, P., Gajjar, A., 2015. Optimization of Astaxanthin microencapsulation in hydrophilic carriers using response surface methodology. Arch. Pharm. Res. https://doi.org/10.1007/s12272-015-0693-5.

Pan, L., Wang, H., Gu, K., 2018. Nanoliposomes as vehicles for astaxanthin: characterization, in vitro release evaluation and structure. Molecules 23, 2822. https://doi.org/10.3390/molecules23112822.

Ponto, T., Latter, G., Luna, G., Leite-Silva, V.R., Wright, A., Benson, H.A.E., 2021. Novel self-nano-emulsifying drug delivery systems containing astaxanthin for topical skin delivery. Pharmaceutics 13. https://doi.org/10.3390/pharmaceutics13050649.

Pouton, C.W., 2000. Lipid formulations for oral administration of drugs: non-emulsifying, self-emulsifying and 'self-microemulsifying' drug delivery systems. Eur. J. Pharm. Sci. 11, S93–S98. https://doi.org/10.1016/S0928-0987(00)00167-6.

Pu, J., Bankston, J., Sathivel, S., 2011. Developing microencapsulated flaxseed oil containing shrimp (Litopenaeus setiferus) astaxanthin using a pilot scale spray dryer. Biosyst. Eng. 108, 121–132. https://doi.org/10.1016/j.biosystemseng.2010.11.005.

Quan, G., Niu, B., Singh, V., Zhou, Y., Wu, C.-Y., Pan, X., Wu, C., 2017. Supersaturable solid self-microemulsifying drug delivery system: precipitation inhibition and bioavailability enhancement. Int. J. Nanomed. 12, 8801–8811. https://doi.org/10.2147/IJN.S149717.

Sharma, T., Jain, A., Kaur, R., Saini, S., Katare, O., Singh, B., 2020. Supersaturated LFCS type III self-emulsifying delivery systems of sorafenib tosylate with improved biopharmaceutical performance: QbD-enabled development and evaluation. Drug Deliv. Transl. Res. 10, 839–861. https://doi.org/10.1007/s13346-020-00772-x.

Shen, X., Fang, T., Zheng, J., Guo, M., 2019. Physicochemical properties and cellular uptake of astaxanthin-loaded emulsions. Molecules 24. https://doi.org/10.3390/molecules24040727.

Shepard, K.B., Adam, M.S., Morgen, M.M., Mudie, D.M., Regan, D.T., Baumann, J.M., Vodak, D.T., 2020. Impact of process parameters on particle morphology and filament formation in spray dried Eudragit L100 polymer. Powder Technol. 362, 221–230. https://doi.org/10.1016/j.powtec.2019.12.013.

Shikov, A.N., Flisyuk, E.V., Obluchinskaya, E.D., Pozharitskaya, O.N., 2020. Pharm. Marine-Derived Drugs 18, 557.

Silva, L.A.D., Almeida, S.L., Alonso, E.C.P., Rocha, P.B.R., Martins, F.T., Freitas, L.A.P., Taveira, S.F., Cunha-Filho, M.S.S., Marreto, R.N., 2018. Preparation of a solid self-microemulsifying drug delivery system by hot-melt extrusion. Int. J. Pharm. 541, 1–10. https://doi.org/10.1016/j.ijpharm.2018.02.020.

Singh, D., Singh, A.P., Singh, D., Kesavan, A.K., Tiwary, A.K., Bedi, N., 2021. Polymeric precipitation inhibitor–based solid supersaturable SMEDD formulation of canagliflozin: improved bioavailability and anti-diabetic activity. J. Pharm. Innov. 16, 317–336. https://doi.org/10.1007/s12247-020-09445-1.

Su, W., Polyakov, N.E., Xu, W., Su, W., 2021. Preparation of astaxanthin micelles self-assembled by a mechanochemical method from hydroxypropyl β-cyclodextrin and glyceryl monostearate with enhanced antioxidant activity. Int. J. Pharm. 605, 120799 https://doi.org/10.1016/j.ijpharm.2021.120799.

Sun, R., Xia, N., Xia, Q., 2020. Non-aqueous nanoemulsions as a new strategy for topical application of astaxanthin. J. Dispers. Sci. Technol. 41, 1777–1788. https://doi.org/10.1080/01932691.2019.1635027.

Thongrangsalit, S., Phaechamud, T., Lipipun, V., Ritthidej, G.C., 2015. Bromocriptine tablet of self-microemulsifying system adsorbed onto porous carrier to stimulate lipoproteins secretion for brain cellular uptake. Colloids Surf. B 131, 162–169. https://doi.org/10.1016/j.colsurfb.2015.04.058.

Tzanova, M., Argirova, M., Atanasov, V., 2017. HPLC Quantification of astaxanthin and canthaxanthin in Salmonidae eggs. Biomed. Chromatogr. 31, e3852. https://doi.org/10.1002/bmc.3852.

United States Pharmacopeia and National Formulary (USP 38-NF 33), 2015. United States Pharmacopeial Convention.

Viera, I., Pérez-Gálvez, A., Roca, M., 2018. Bioaccessibility of marine carotenoids. Mar. Drugs 16. https://doi.org/10.3390/md16100397.

Vlachos, N., Skopelitis, Y., Psaroudaki, M., Konstantinidou, V., Chatzilazarou, A., Tegou, E., 2006. Applications of Fourier transform-infrared spectroscopy to edible oils. Anal. Chim. Acta 573-574, 459–465. https://doi.org/10.1016/j.aca.2006.05.034.

Wan, H., Liu, D., Yu, X., Sun, H., Li, Y., 2015. A Caco-2 cell-based quantitative antioxidant activity assay for antioxidants. Food Chem. 175, 601–608. https://doi.org/10.1016/j.foodchem.2014.11.128.

Wang, L., Yan, W., Tian, Y., Xue, H., Tang, J., Zhang, L., 2020. Self-microemulsifying drug delivery system of phillygenin: formulation development, characterization and pharmacokinetic evaluation. Pharmaceutics 12, 130. https://doi.org/10.3390/pharmaceutics12020130.

Wang, Q., Zhao, Y., Guan, L., Zhang, Y., Dang, Q., Dong, P., Li, J., Liang, X., 2017. Preparation of astaxanthin-loaded DNA/chitosan nanoparticles for improved cellular uptake and antioxidation capability. Food Chem. 227, 9–15. https://doi.org/10.1016/j.foodchem.2017.01.081.

Yamashita, E., 2013. Astaxanthin as a medical food. Funct. Food Health Dis. 3, 254–258. https://doi.org/10.31989/ffhd.v3i7.49.

Yang, C., Zhang, H., Liu, R., Zhu, H., Zhang, L., Tsao, R., 2017. Bioaccessibility, cellular uptake, and transport of astaxanthin isomers and their antioxidative effects in human intestinal epithelial Caco-2 Cells. J. Agric. Food Chem. 65, 10223–10232. https://doi.org/10.1021/acs.jafc.7b04254.

Yang, Y., Kim, B., Lee, J.Y., 2013. Astaxanthin structure, metabolism, and health benefits. J. Hum. Nutr. Food Sci. 1, 1–1003.

Yeom, D.W., Chae, B.R., Kim, J.H., Chae, J.S., Shin, D.J., Kim, C.H., Kim, S.R., Choi, J.H., Song, S.H., Oh, D., 2017. Solid formulation of a supersaturable self-microemulsifying drug delivery system for valsartan with improved dissolution and bioavailability. Oncotarget 8, 94297. https://doi.org/10.18632/oncotarget.21691.

Zhao, N., Augsburger, L.L., 2005. The influence of swelling capacity of superdisintegrants in different pH media on the dissolution of hydrochlorothiazide from directly compressed tablets. AAPS PharmSciTech 6, E120–E126. https://doi.org/10.1208/pt060119.

Zin, M.M.K., Boonkanokwong, V., 2021. Systematic development by the design-of-experiment approach and physicochemical evaluations of the optimized self-microemulsifying astaxanthin delivery system. Thai J. Pharm. Sci. 45, 508–526.

Zuluaga, M., Barzegari, A., Letourneur, D., Gueguen, V., Pavon-Djavid, G., 2017. Oxidative stress regulation on endothelial cells by hydrophilic astaxanthin complex: chemical, biological, and molecular antioxidant activity evaluation. Oxid. Med. Cell. Longev., 8073798 https://doi.org/10.1155/2017/8073798, 2017.